Author Manuscript

Author Manuscript

Author Manuscript

Author Manuscript

HHS Public Access

Author manuscript

Biofabrication. Author manuscript; available in PMC 2020 May 22.

Published in final edited form as:

Biofabrication. ; 11(4): 045005. doi:10.1088/1758-5090/ab25f9.

Thermal inkjet bioprinting triggers the activation of the VEGF pathway in human microvascular endothelial cells *in vitro*

Luis H Solis[1,2], **Yoshira Ayala**[2], **Susana Portillo**[2], **Armando Varela-Ramirez**[2], **Renato Aguilera**[2], **Thomas Boland**[1]

[1]Department of Metallurgical, Materials, and Biomedical Engineering, University of Texas at El Paso, El Paso, TX 79968, United States of America

[2]Border Biomedical Research Center, Department of Biological Sciences, The University of Texas at El Paso, El Paso, TX 79968, United States of America

Abstract

One biofabrication process that has gained tremendous momentum in the field of tissue engineering and regenerative medicine is cell-printing or most commonly bioprinting. We have shown that thermal inkjet bioprinted human microvascular endothelial cells were recruited or otherwise involved in the formation of microvasculature to form graft-host anastomoses upon implantation. The present study aims to quantify and characterize the expression and activation of specific cytokines and kinases *in vitro*. Morphological characteristics demonstrate elongated protrusions of TIB-HMVECs at 5–6 times the size of manually pipetted cells. Moreover, annexin V-FITC and propidium iodide apoptosis assay via flow cytometry demonstrated a 75% apoptosis among printed cells as compared to among control cells. Cell viability at a 3 d incubation period was significantly higher for printed cells as compared to control. Milliplex magnetic bead panels confirmed significant overexpression of HSP70, IL-1α, VEGF-A, IL-8, and FGF-1 of printed cells compared to control. In addition, a Human phospho-kinase array displayed a significant over activation of the heat-shock proteins HSP27 and HSP60 of printed cells compared to the manually seeded cells. Collectively, it is suggested that the massive appearance of capillary blood vessels upon implantation that has been reported elsewhere may be due to the activation of the HSP-NF-κB pathway to produce VEGF. This cell activation may be used as a new strategy for vascularization of tissue engineered constructs which are in high demand in regenerative medicine applications.

Keywords

thermal inkjet bioprinting; cytokines; angiogenesis; heat-shock proteins; NF-kB pathway; VEGF release; apoptosis

tboland@utep.edu.

Author Manuscript Author Manuscript Author Manuscript Author Manuscript

1. Introduction

Tissue engineering is a multidisciplinary practice focusing on developing new ways to repair, regenerate, or replace injured tissues and organs. Using a combination of cells, growth factors, biomaterials, and engineering technologies, artificial tissues can be created to replace their injured counterparts. One biofabrication process that has gained tremendous momentum is cell-printing or bioprinting.

Bioprinters are advantageous in that they deposit cells and biomaterials in precise spatial arrangements to enhance cell–cell communication, decrease cell migration time in populating a tissue construct, and allow for the creation of artificial structures that closely resemble *in vivo* tissues and organs [1]. The three main types of bioprinters are inkjet, microextrusion, and laser-assisted printing. Comprehensive reviews on these bioprinters have been recently published [2–6]. Most, if not all of the printing modalities involve heat generation, be it via laser, heated nozzles, or friction as cells are forced through narrow orifices. Little is known, however, about the direct effects that bioprinting causes on cells, e.g. heat-, shear-stress. Very few studies focused on analyzing the biochemical pathways that may or may not be activated by this heat. In this paper, we study the effect of heat generated from a thermal inkjet bioprinter that was developed in our laboratory [7]. In previous work, thermal inkjet bioprinted (TIB) Chinese Hamster Ovary (CHO) cells had a viability of 89% and interestingly the process also caused the formation of pores to appear on the cell membrane [8]. We have also demonstrated that TIB-human microvascular endothelial cells (HMVECs) were recruited or otherwise involved in the formation of microvasculature in host animals [9, 10]. Markers for HMVECs in immunocompromised mice verified anastomoses of vascular structures between graft and host [11].

While it is important to conduct studies that characterize the interaction between host and implanted bioprinted constructs, it is also important to understand the effects of the printing process in order to improve the engineering design of these tissues or to improve printer designs. Cells are fast adapting to their environment and they change intracellular structures, proliferation, movement, and differentiation in response to external mechanical stimuli [1, 12]. In addition, changes in cell morphology due to mechanical injury may cause changes in downstream cellular development [1, 13]. We hypothesize that the heat and the shear mechanical forces experienced by the cells during the TIB process could have longer lasting effects on the cells ready to be transplanted. For these reasons, we sought to investigate whether TIB-HMVECs are being activated to secrete cytokines in their supernatant and/or to phosphorylate kinases intracellularly. The heat from the TIB process may cause HMVECs to release and activate specific angiogenic cytokines and kinases resulting in the massive formation of capillary blood vessels upon implantation via a heat-shock protein (HSP) regulated mechanism. It has been demonstrated that HSP27 and other HSPs regulate and induce angiogenesis, especially tumor angiogenesis [14, 15]. Eighteen HSP90 inhibitors have recently entered the clinic as anti-cancer drugs [16], and HSP70 antagonists are explored as adjuvants [17]. However, in the field of tissue engineering and particularly bioprinting, activation of the angiogenic pathway via HSP may be the desired response as vascularization and host integration of implants remains a considerable challenge. In the

Author Manuscript Author Manuscript Author Manuscript Author Manuscript

present study, we demonstrate that TIB promotes the expression and activation of cytokines and kinases. Additionally, HSPs appear to be involved in activating the angiogenic pathway.

2. Methods

2.1. Cell culture

Primary adult Human dermal microvascular endothelial cells (HMVECs) (Lonza) were cultured in endothelial cell growth basal medium-2 (EBM-2, Lonza) supplemented with an endothelial growth media (EGM-2, Lonza) kit containing 10 ml fetal bovine serum (FBS); 0.2 ml hydrocortisone; 0.2 ml basic Human fibroblast growth factor-basic (hFGF-B); 0.5 ml vascular endothelial growth factor (VEGF); 0.5 ml of complete human insulin like growth factor-1 with substitution of Arg for Glu^3 (R^3-IGF-1); 0.5 ml ascorbic acid; 0.5 ml Human epidermal growth factor (hEGF); 0.5 ml gentamicin sulfate-amphotericin (GA-100; and 0.5 ml heparin per 100 ml EBM-2). Cell cultures were maintained at 37 °C in a 5% CO_2 environment. Passaged at 80% confluency and were used up to passage nine for the present experiments.

2.2. Bioink and bioprinting preparation

With the use of a thermal inkjet printer developed in our laboratory [7], a corresponding bioink solution was made with 0.13 M $CaCl_2$ in 18 mOhm deionized water (milli-Q) and sterilized via syringe filtration giving a final osmolality concentration of 300 mOsm kg^{-1}. HMVECs were trypsinized, counted, and mixed in the bioink solution to obtain a final concentration of 2×10^5 cells in 800 μl. 100 μl of the $CaCl_2$/HMVECs solution was loaded inside a modified printer cartridge and printed into the corresponding petri dish pre-filled with 6 ml of complete EBM-2 media.

2.3. Cell morphology analysis

Cell morphology of TIB and manually pipetted (MP) cells were observed using an Olympus IX71 micro-scope at 10× (bright field) and 20× (phase contrast) after a 24 h incubation period. Images were taken with an Olympus DP72 digital camera with a 12.5 megapixel resolution. Images were further processed using PowerPoint with a color tone of 6500 K, 100% color saturation, 0% brightness and contrast, and a 50% sharpness.

2.4. Annexin V apoptosis analysis

An Annexin A5 fluorescein isothiocyanate (FITC)/propidium iodide (PI) Kit (Beckman Coulter) was used for detection of externalized phosphatidylserine (an early event of apoptosis induction) on TIB and MP cells after a 24 h incubation period. HMVECs in complete media with 1 mM H_2O_2 used as positive control. Briefly, 2×10^5 cells were TIB and MP into 60 × 15 mm Petri dishes containing 6 ml of complete EBM-2/EGM2 media and incubated for 24 h. After 24 h, the supernatant with the floating dead cells was collected, the live attached cells were trypsinized, collected, and added to the initial supernatant containing the dead cells. Cells were washed with ice-cold 1X PBS and resuspended into a 106 μl from a 1060 μl master mix (1000 μl binding buffer, 10 μl Annexin A5-FITC, and 50 μl PI) before a 15 min incubation in the dark. Finally, 300 μl of the kit's binding buffer was added to each tube and flow cytometric analysis was conducted within 30 min. Samples were analyzed in

Author Manuscript Author Manuscript Author Manuscript Author Manuscript

triplicates on a GALLIOS flow cytometer (Beckman Coulter). Debris was excluded by applying gates on side scatter versus forward scatter histograms (data not shown). For all assays 10 000 events (cells) were acquired. The total percentage of apoptotic cells is demarcated as the sum of both early and late apoptotic subpopulations percentages; annexin V-FITC positive cells [18, 19]. All flow cytometric data were analyzed using Kaluza software (Beckman Coulter).

2.5. Cell viability propidium iodide exclusion assay

HMVEC viability percentages were quantified in triplicates by a GALLIOS flow cytometer (Beckman Coulter) with the use of a propidium iodide (PI) exclusion assay [20, 21]. Briefly, HMVECs were TIB and MP into a 6-well plate at a final seeding density of 40 000 cells/well in 6 ml of EBM-2/EGM-2 complete media. Cell viability was then determined after a 3 and 7 d incubation period. At each incubation period, the supernatant containing all floating dead cells were collected. Live cells were then trypsinized and collected together with the initial supernatant. The complete cell samples were then stained with 5 μm ml^{-1} of PI, incubated for 15 min in the dark, and analyzed via flow cytometry. Unstained cells were used as controls to fine-tune the detector voltages, and to modify the compensation values resulting in a gated ovoid shape of living cells. For all assays, 10 000 events (cells) were acquired per sample and analyzed using the Kaluza software (Beckman Coulter).

2.6. Multiplex cytokine analysis

Multiplex magnetic bead immunoassays were performed on 0, 6, 12, and 24 h supernatants collected from TIB and MP HMVECs from 60 × 15 ml Petri dishes containing 6 ml of complete media. HMVECs left in the $CaCl_2$ bioink for 1 h at room temperature were used as a control and heat-shocked HMVECs passed through a Pasteur pipette heated with a soldering iron at 300 °C to mimic the bioprinting process were used as a negative control. Conditioned media was centrifuged for 5 min at 4000 rpm on a tabletop microcentrifuge at room temperature and divided into aliquots of 1.0 ml for storage at −4°C until analysis. Supernatants were analyzed with the Milliplex Human Sepsis Panel 2 Magnetic Bead Panel with HSP70, interleukin-1 alpha (IL-1α), and interleukin-8 (IL-8). Supernatants were also examined with the Milliplex map Human angiogenesis/growth factor magnetic bead panel 1 with Angiopoietin-2 (Ang-2), FGF-1, and VEGF-A (Millipore Sigma) according to the manufacturer's protocol with the use of the Luminex xMAP technology [22]. Briefly, in a 96-well plate, 200 μl of Assay Buffer was added, the plate was shaken for 10 min, and the buffer was discarded. Twenty-five microliters of the standards, 25 μl of the Assay Buffer, 25 μl of stock solution, 25 μl of supernatant from cells into the corresponding wells, and 25 μl of the bead mixture were added. The plate was foil-wrapped and incubated overnight with shaking at 4 °C (Milliplex Human Sepsis Panel 2 was incubated for 2 h at room temperature). The supernatant was removed and washed three times (washed twice for the Human sepsis panel 2) with 200 μl of wash buffer. Next, 25 μl of the detection antibodies were added, the plate was foil-wrapped, and incubated for 1 h at room temperature with shaking. Without aspirating the supernatant, 25 μl of streptavidin-phycoerythrin was added, the plate was foil-wrapped, and incubated at room temperature for 30 min. The contents were discarded and washed three times (twice for the Human Sepsis Panel 2) with 200 μl of the wash buffer. Finally, 100 μl of the sheath fluid was added and the plate was read on a

Author Manuscript Author Manuscript Author Manuscript Author Manuscript

MAGPIX Instrument. Median fluorescent intensity (MFI) data using a 5-parameter curve-fitting method was used to measure analyte concentrations. The results from the samples were analyzed using the Luminex xPONENT Software Version 4.2 Build 1324.

2.7. Proteome phospho-kinase array

HMVECs from three T-75 flasks at ~80% confluency were TIB and manually (pipetted) seeded into a 100 × 15 mm Petri dish and incubated for 12 h at 37 °C, 5% CO_2. Then, cells were washed with PBS, lysed in the presence of 1 mM phenylmethylsulfonyl fluoride, 5 μg ml^{-1} aprotinin, 2 μg ml^{-1} leupeptin, and 1 μg ml^{-1} pepstatin A proteases inhibitors and the resulting supernatant was clarified by centrifugation (14 000 rpm, 5 min, 4 °C). Protein concentration was determined by the bicinchoninic acid method (Pierce). Equal concentrations of protein were analyzed using the Proteome Profiler Human Phospho-Kinase Array Kit (R&D Systems #ARY003B) according to the manufacturer's protocol. In this array, phosphorylation of 43 kinases and 2 related proteins were examined. Analytes and phosphorylation sites included: p38α (T180/Y182), extracellular signal regulated kinase 1/2 (ERK1/2) (T202/Y204, T185/Y187), jun N-terminal kinase 1/2/3 (JNK 1/2/3) (T183/Y185, T221/Y223), glycogen synthase kinase 3α/β (GSK-3α/β) (S21/S9), p53 (S392), epidermal growth factor receptor (EGF R) (Y1086), mitogen- and stress-activated protein kinase 1/2 (MSK1/2) (S376/S360), adenosine monophosphate-activated protein kinase α1 (AMPKα1) (T183), protein kinase B 1/2/3 (AKT 1/2/3) (S473), protein kinase 1/2/3 AKT 1/2/3 (T308), p53 (S46), target of rapamycin (TOR) (S2448), cAMP response element-binding protein (CREB) (S133), heat-shock protein 27 (HSP27) (S78/S82), adenosine monophosphate-activated protein kinase α2 (AMPKα2) (T172), β-Catenin, p70 S6 Kinase (T389), p53 (S15), protein kinase c-Jun (c-Jun) (S63), proto-oncogene tyrosine-protein kinase (Src) (Y419), protein kinase Lyn (Lyn) (Y397), protein kinase Lck (Lck) (Y394), signal transducer and activator of transcription proteins 2 (STAT2) (Y689), signal transducer and activator of transcription proteins 5a (STAT5a) (Y694), p70 S6 Kinase (T421/S424), ribosomal s6 kinase 1/2/3 (RSK1/2/3) (S380/S386/S377), endothelial nitric oxide synthase (eNOS) (S1177), protein kinase Fyn (Fyn) (Y420), protein kinase Yes (Yes) (Y426), protein kinase Fgr (Fgr) (Y412), signal transducer and activator of transcription proteins 6 (STAT6) (Y641), signal transducer and activator of transcription proteins 5b (STAT5b) (Y699), signal transducer and activator of transcription proteins 3 (STAT3) (Y705), p27 (T198), phospholipase C-γ1 (PLC-γ1) (Y783), protein kinase Hck (Hck) (Y411), checkpoint kinase-2 (Chk-2) (T68), protein kinase FAK (FAK) (Y397), platelet-derived growth factor receptor β (PDGF Rβ) (Y751), signal transducer and activator of transcription proteins a/b (STAT5a/b) (Y694/Y699), signal transducer and activator of transcription proteins 3 (STAT3) (S727), lysine deficient protein kinase 1 (WNK1) (T60), proline-rich tyrosine kinase 2 (PYK2) (Y402), proline-rich AKT substrate (PRAS40) (T246), and heat-shock protein 60 (HSP60). Nitrocellulose membranes were visualized by enhanced chemiluminescence and x-ray film (Phenix). Densitometric analysis was performed using Image Studio Lite version 5.2.

2.8. Statistical analysis

All values are displayed as the average of triplicate, with their corresponding standard deviations. Statistical significance between two different samples was determined through

Author Manuscript Author Manuscript Author Manuscript Author Manuscript

two-tailed paired Student's *t*-tests, and a *p* value of less than 0.05 was considered statistically significant.

3. Results and discussion

3.1. TIB-HMVECs demonstrate elongating characteristics

After a 24 h incubation period, bright field microscopy images revealed that TIB-HMVECs demonstrate thin and long protuberances as compared to the MP-HMVECs (figure 1). TIB-HMVECs are thin and elongated at 2–3 times longer than the MP. In both 10× and 20× images, one TIB-HMVEC is approximately 5–6 times the size of an MP-HMVEC (figures 1(a) and (c)). Manually pipetted HMVECs, however, convey a thick, short, diamond-shaped body at both 10× and 20× magnification (figures 1(b) and (d)). The elongation process among TIB cells might be due to the activation of these cells. Figure 3 demonstrates that the TIB process had a significant overexpression of VEGF-A and other angiogenic heat-shock proteins and cytokines as compared to MP cells. This response may be due to the heat and shear stress from the TIB process.

3.2. TIB induces cell apoptosis

The effects of the thermal inkjet bioprinting process were assessed by an apoptosis/necrosis protocol through the annexin A5-FITC/PI assay analyzed via flow cytometry. In cells undergoing apoptosis, phosphatidylserine (PtdSer) is translocated to the outer leaflet of the plasma membrane facing the extracellular space [23–26]. Annexin, which has a high affinity for PtdSer, allows for the accurate detection of its externalization via flow cytometry with the aid of FITC. A bar graph and the flow cytometer dot plots of the results are depicted in figure 2. After a 24 h incubation period, approximately 75% of TIB-HMVECs were apoptotic as compared to 22% of the MP cells (figures 2(a)–(c)). Note that HMVECs are very sensitive to manipulation and generally exhibit a lower viability than immortal/transformed cell lines (MP cells in figures 2(a) and (c)). This sensitivity may be because these HMVECs are primary cells and thus short lived. However, in previous studies, TIB-Chinese Hamster Ovary (CHO) cells and neonatal human dermal fibroblasts had a cell viability of 89% [8] and 68% (Data not published), respectively. Additionally, the apoptotic percentages reported in figure 2 were determined by the sum of the dead cells floating in the supernatant as well as the viable cells that were attached to the Petri dish after a 24 h incubation period. Therefore, this analysis is an overall assessment of cell viability. Most studies published to date show live-dead assays of cells attached to scaffolds and are not reporting the percentage of cells that are not attaching. This is typically done because only the scaffolds with bioprinted cells will be used for tissue engineering or other applications. Hydrogen peroxide was used as a positive control for the induction of apoptosis and, as expected, it resulted in a strong PtdSer externalization of 86% (figure 2(d)). Apoptosis induction among TIB-HMVECs may seem relatively high, however, as noted in figure 2(b), HMVECs are very sensitive primary cells resulting in a 67% viability with just trypsinizing and manipulation alone. Thus, findings suggest that the thermal inkjet bioprinting technology elicits some apoptosis in HMVECs which will not attach to the scaffolds and that this needs to be considered when printing scaffolds for tissue engineering or other

Author Manuscript Author Manuscript Author Manuscript Author Manuscript

applications. One would need to increase the cell concentration in the bioink for example or overprint to achieve a desired cell concentration on the scaffold.

3.3. Effects of TIB on cell viability

Cell viability was also measured on day 3 and day 7 post printing with a PI exclusion assay and analyzed via flow cytometry. PI is impermeable to cells with intact cell membranes, however, in cells with ruptured membranes, the PI binds to the DNA rendering the dead cells highly fluorescent [27]. Displayed in figure 3 are a bar graph and dot plots of these flow cytometry results. Figures 3(a) and (c) shows that after a 3 d incubation period, TIB-HMVEC's viability was significantly higher in comparison to MP-HMVECs (92% versus 86% cell viability, respectively). After a 7 d incubation period, however, there was no significant difference in cell viability between TIB and MP cells, figures 3(a) and (d). Figure 3(b) is a dot plot of untreated HMVECs without PI used as a control to determine the gate of viable cells. The reason we see a higher cell viability among TIB-HMVECs might be due to increased secretion of VEGF-A, figure 4(c). VEGF is a potent mitogen that regulates endothelial cell proliferation [28, 29]. At 7 d, these VEGF values might equilibrate to those similar to MP-HMVECs that we see in figures 3(a) and (d). Overall, the high cell viability shown by TIB-HMVECs after a one-week incubation period demonstrates their potential incorporation into tissue engineering and regenerative medicine applications. These results are also similar to previous studies where only cells attached to scaffolds were analyzed with respect to PI permeability.

3.4. TIB induces the expression of cytokines

The 6-panel multiplexed magnetic bead assay categorized the differences in cytokine expression between TIB and MP-HMVECs. The heating element in the inkjet cartridge will heat to approximately 300 °C for 2 μs, then cool again for 200 μs. This heat creates a bubble that then bursts resulting in the ejection of bioink droplets and the cells in the ink may be exposed to an elevated temperature. However, the temperature of the ink droplets does not exceed ten degrees above room temperature [30]. In addition to heat, cells are exposed to mechanical forces as they are expelled through the nozzle orifices. Parameters for thermal inkjet printers include a nozzle diameter of 40–100 μm, droplet volumes of 50–500 PL, operating frequencies of 3–25 kHz, and droplet velocity of 3–15 ms^{-1} [31]. The cytokine expression was measured after a 12 h incubation period for both treatment groups.

Bar graphs in figure 3 show the median fluorescent intensity (MFI) as it corresponds to the comparative expression levels of six specifically selected cytokines, including heat-shock protein 70 (HSP70), interleukin 1 (IL-1α), vascular endothelial growth factor A (VEGF-A), interleukin 8 (IL-8), fibroblast growth factor 1 (FGF-1), and angiopoietin 2 (Ang-2), between TIB and MP-HMVECs. The MFI values for IL-1α and FGF-1 may appear low and insignificant in comparison to the other four cytokines, however, when we took MFI readings of the EBM-2 media supplemented with an EGM-2 growth factor kit (Lonza), we found similar trends in their MFI values: IL-8, 12.5; IL-1α, 38.5; FGF-1, 106.75; Ang-2, 163; HSP70, 306; and VEGF-A, 6623. As noted, media alone (devoid of cells) contains great amounts of VEGF-A and low levels of IL-1α, IL-8, FGF-1, Ang-2, and HSP70. Interestingly, the amount of HSP70 found in the EMB-2/EGM-2 complete media alone was

Author Manuscript Author Manuscript Author Manuscript Author Manuscript

surpassed by over 7 times among TIB cells and was almost doubled in the MP cells. As a result, HSP70 was significantly overexpressed among TIB-HMVECs as compared to the MP cells (figure 3(a)). This confirms that the TIB process is eliciting a heat shock response resulting in the production of HSP70. Additionally, IL-1α increased over three times the amount in media alone among TIB cells and increased slightly among MP cells with an overall significant overexpression between both treatment groups (figure 3(b)). This further confirms the cell-based injury from TIB. IL-1α is a well-known inflammatory cytokine that is expressed in response to trauma [32]. Moreover, IL-1α has been shown to promote the production of HSP70 family proteins [33]. This also proves that pipetting cells manually causes minor cellular damage. The expression of VEGF-A in figure 3(c) was more than doubled among TIB cells in comparison to their EBM-2/EGM-2 complete media values and may have been consumed by the MP cells. The observed VEGF-A expression may not only be due to the shear stress from the printing process [34], but also from the protective effects that HSP70 has on VEGF production [35]. Figure 3(d) shows the expression of IL-8 which was almost 700 times fold for TIB and over 400 times fold for MP cells in comparison to their complete media values. Furthermore, IL-8 was significantly overexpressed among TIB cells in comparison to MP cells. IL-8, another pro-angiogenic cytokine [33], increases proliferation, migration, and angiogenesis among ECs [36, 37] by inducing VEGF secretion [38]. The expression of FGF-1 among TIB cells was similar to the value in the complete media, however, among MP cells, FGF-1 was completely depleted (figure 3(e)). Also, FGF-1 was overexpressed significantly in TIB cells in comparison to MP cells. Finally, the expression of Ang-2 among TIB cells was seven times the complete media values and over four times among the MP cells (figure 3(f)). However, there were no significant differences in expression between both treatment groups. It may be possible that Ang-2 may have a synergistic effect with VEGF-A in our experiment [39, 40]. It has been demonstrated that Ang-1 is the key angiopoietin in EC migration, survival, and vessel development and Ang-2 is its antagonist, however, along with VEGF, Ang-2 has proven to elicit angiogenic effects [41].

In a previous experiment, we measured cytokine expression at 0, 6, 12, and 24 h periods and found that the most cytokine expression occurred at 12 h (data not shown). For this reason, the 12 h incubation period was chosen for the present experiment. To test if the $CaCl_2$ bioink had any effect on the expression of these cytokines, a control group consisting of HMVECs left in the bioink for an hour at room temperature was examined. As expected, minimal values of cytokine expression were lower than their EBM-2/EGM-2 complete media (data not shown). We also examined if the cell contents from ruptured HMVECs were releasing vast amounts of the selected cytokines. To test for this, we included a negative control consisting of heat shocked HMVECs ejected from a Pasteur pipette heated with a solder iron to 300 °C that resulted in complete cell death. Once again, minimal values of cytokine expression were detected in comparison to their EBM-2/EGM-2 complete media (data not shown). This test proved that cytokine expression is an active and not a passive process.

We are confident that the TIB process activates or promotes angiogenic signals in HMVECs. We purposely selected these six cytokines due to their potent angiogenic effects. HSP70–1A, a member of the HSP70 family, binds to the surface of endothelial cells (ECs), activates HUVEC migration and tube formation *in vitro,* promotes vascularity formation *in vivo* [42],

Author Manuscript Author Manuscript Author Manuscript Author Manuscript

and is required for IL-5 induced angiogenic responses [43]. FGF-1 regulates cell differentiation, proliferation, survival, and angiogenesis [44]. To date, VEGF-A is the most potent pro-angiogenic cytokine. It promotes proliferation, tube formation, and sprouting of ECs [45, 46]. The TIB process did induce the expression of six potent angiogenic cytokines and these may be the reason behind the differences in morphological differences between the TIB and MP-HMVECs as depicted in figure 1.

3.5. TIB activates the phosphorylation of kinases

To determine the biological mechanism by which TIB activates HMVECs, a proteome phospho-kinase array of 45 kinases involved in cell proliferation, survival, angiogenesis, migration, and stress was performed. The bar graph depicted in figure 4(a) demonstrates that signal transducers and activators of transcription 3 (STAT3), tyrosine-protein kinase (Fyn), target of rapamycin (TOR), and protein kinase B (AKT1/2/3) were significantly over activated in MP cells as compared to TIB cells. All four of these kinases are involved in endothelial cell (EC) proliferation, migration, and regulation of angiogenesis by VEGF [47–51]. Similarly, the bar graph in figure 4(b), shows that tyrosine-protein kinase (Yes), cyclic amp response element-binding protein (CREB), Src, cell cycle checkpoint kinase 2 (Chk2), AMP-activated protein kinase (AMPKα1), c-Jun, focal adhesion kinase (FAK), glycogen synthase kinase (GSK-3α/β), and c-Jun N-terminal kinase (JNK1/2/3) were over activated significantly in MP-HMVECS as compared to the TIB cells. Src and Yes are involved in VEGF induced cell migration and mitogenic signaling [49, 52]. Chk2 mediates the cell cycle and apoptosis [53], and AMPKα1 regulates metabolism and the expression of β-Catenin [54]. CREB and GSK-3α/β are involved in cell proliferation [55, 56] while JNK 1/2/3 and c-JUN are also involved in angiogenesis [57, 58].

Since angiogenesis is heavily determined by EC proliferation, elongation, and migration, it might be interesting to determine if the TIB process influences any of these three angiogenic processes. Straight vessels formed *in vitro* were found to be the result of proliferating ECs under strain [60]. The morphologic characteristics of the TIB-HMVECs seem to follow this result as they also appear to be elongated in a straight form, figures 1(a) and (c). Tumors, on the other hand, contain tortious blood vessels *in vivo* due to the increased proliferation and decreased migration of ECs [61]. Increased branching due to high EC proliferation, however, results in anastomoses of nonfunctional blood vessels that eventually deteriorate [62]. As a blood vessel forms, ECs proliferate according to their cell cycle. Cells at the end or tips of developing vessels elongate as a sensing mechanism. The cells that remain in the middle of the vessel form the stalk and deactivate or go into a quiescent mode. The same occurs when vessels anastomose, the proliferating cells at the tip touch the stalk of a vessel and as they fuse, the mature cells go into a quiescent mode [61]. This mechanism may be what we found among the TIB-HMVECs. As these cells first become activated and elongate, they may fall under the quiescent state, where they do not proliferate nor migrate anymore by turning off their respective kinases as we show here in figures 4(a) and (b).

Most interestingly, and confirmed in the proteome array, the TIB process caused a significant over activation of heat-shock protein 27 and 60 (figure 4(b)) which have also been proven to play angiogenic roles [63]. It is well established that the nuclear factor

Author Manuscript Author Manuscript Author Manuscript Author Manuscript

kappa-light-chain enhancer of activated B cells (NF-κB) activation from HSP27 leads to the secretion of IL-8 and VEGF [64]. In addition, HSP27 actives toll-like receptors (TLRs) on ECs to induce NF-kB activation, resulting in VEGF-mediated EC migration and angiogenesis [65]. HSP27 regulates p53 signaling and decreases cellular senescence [66]. This may be another reason for the elongated morphological characteristics from figure 1 and the spike of VEGF-A in figure 4. Similarly, HSP60 has also been shown to promote angiogenesis [67]. HSP60 has been shown to be localized in the mitochondria of unstressed HUVECs, however, in stressed HUVECs, HSP60 was found on the cytoplasm and surface membrane [68]. We hypothesize that HSP27, HSP60, and HSP70 are being produced as a result of stress induced from the TIB process causing an autocrine and paracrine effect on ECs to produce VEGF-A. It is possible that as these HSPs get externalized via exosomes [69–71], they bind their TLRs and possibly induce angiogenic pathways such as the NF-κB to produce VEGF, however, this hypothesis remains to be proven. A schematic of how the TIB process triggers the activation of the VEGF pathway is depicted in figure 6.

The effects observed in our study may not only be specific to thermal inkjet printers but might also occur in laser-based direct-write printing, electrospinning techniques for cell patterning and possibly extrusion-based systems when small diameter nozzles are used. Laser-based direct-write printing technologies include laser-induced forward transfer (LIFT), absorbing film-assisted laser-induced forward transfer (AFA-LIFT), biological laser processing (BioLP), matrix-assisted pulsed laser evaporation direct writing (MAPLE DW), and laser-guided direct writing (LG DW) [75]. Cell electrospinning consists of electrospun cell-laden threads within a specific biosuspension [76]. In laser-based direct-write cell patterning, the laser heats the laser absorption layer, causing the formation of a bubble which collapses, resulting in the specified pattern. Cell viability regarding cell acceleration and deceleration as the cell droplet forms and lands on the substrate is discussed. However, there is no mention of the heat stress induced by the laser [75]. Regarding cell electrospinning, cell viability was found to be 25%, similar to other findings [77]. Among solid freeform fabrication-based direct cell writing, dispensing pressure and nozzle size was found to induce mechanical cell membrane damage [1].

As we have documented, all these different cell manipulations or patterning techniques for the purposes of biofabricating living systems induce some form of stress or significant cell death. For this reason, we ought to characterize the expression and activation of various cytokines and kinases among other biofabrication techniques to see if we are indeed creating the desired effects upon implantation. There is also the possibility that the bioprinting process changes the intracellular structures of the cells, leading to the physiological change of cells and possibly inducing cell transformation or uncontrolled cell growth. As a result, our focus towards new biofabricating methods should involve designing novel cell manipulation techniques that promote less heat and mechanical induced cellular trauma and developing heat-resistant bioinks or cell encapsulating methods in order to minimize the downstream damaging effects from the bioprinting process.

Author Manuscript Author Manuscript Author Manuscript Author Manuscript

4. Conclusion

In conclusion, we have demonstrated that TIB-HMVECs overexpressed and activated specific cytokines and HSPs that may play an angiogenic role. This bioprinting process is a repeatable, feasible, and inexpensive technique to develop angiogenic scaffolds. Due to the significant progress in creating artificial tissues and constructs with geometric precision, the formation of anastomosis and functional vascular networks remains a tremendous challenge [78]. We believe that the TIB cell activation process may be used as a new strategy for vascularization of tissue engineered constructs, which are in high demand in regenerative medicine and drug testing applications. Our future work involves performing siRNA gene knockdown experiments to confirm our observations and fine tuning our system to behave in an angiogenic fashion. Additionally, we would like to perform a comparative analysis between different cell patterning techniques and determine whether they have similar effects.

Acknowledgments

This work was funded by National Institute of General Medical Sciences linked Award Numbers RL5GM118969, TL4GM118971, and UL1GM118970. The work was also supported by the PREM Center for Energy and Biomaterials through the National Science Foundation award #1827745. LHS is supported by the Research Initiatives for Scientific Enhancement (RISE) program, NIH-NIGMS (Grant No. 5R25GM069621–15). The authors would also like to thank Denisse Gutierrez and the Border Biomedical Research Center (BBRC) at the University of Texas at El Paso for their quality services and facilities provided. The BBRC is supported by the NIH-NIMHD-RCMI (Grant No. 5G12MD007592).

References

[1]. Chang R, Nam J and Sun W 2008 Effects of dispensing pressure and nozzle diameter on cell survival from solid freeform fabrication–based direct cell writing Tissue Eng. A 14 41–8

[2]. Murphy SV and Atala A 2014 3D bioprinting of tissues and organs Nat. Biotechnol 32 773–85 [PubMed: 25093879]

[3]. Li J, Chen M, Fan X and Zhou H 2016 Recent advances in bioprinting techniques: approaches, applications and future prospects J. Transl. Med 14 271–86 [PubMed: 27645770]

[4]. Zhang YS et al. 2017 3D bioprinting for tissue and organ fabrication Ann. Biomed. Eng 45 148–63 [PubMed: 27126775]

[5]. Ringeisen BR, Pirlo RK, Wu PK, Boland T, Sun W, Hamid Q, Huang Y and Chrisey DB 2013 Cell and organ printing turns 15: diverse research to commercial transitions MRS Bull 38 834–43

[6]. Ji S and Guvendiren M 2017 Recent advances in bioink design for 3D bioprinting of tissues and organs Frontiers Bioeng. Biotechnol 5 23–31

[7]. De Maria C, Rincon J, Duarte AA, Vozzi G and Boland T 2013 A new approach to fabricate agarose microstructures Polym. Adv. Technol 24 895–902

[8]. Cui X, Dean D, Ruggeri ZM and Boland T 2010 Cell damage evaluation of thermal inkjet printed chinese hamster ovary cells Biotechnol. Bioeng 106 963–9 [PubMed: 20589673]

[9]. Yanez M, Rincon J, Dones A, De Maria C, Gonzales R and Boland T 2015 *In vivo* assessment of printed microvasculature in a bilayer skin graft to treat full-thickness wounds Tissue Eng. A 21 224–33

[10]. Burg KJL, Dréau D and Burg T 2017 Engineering 3D Tissue Test Systems (Boca Raton, FL: CRC Press) (10.1201/9781315118260)

[11]. Rouwkema J and Khademhosseini A 2016 Vascularization and angiogenesis in tissue engineering: beyond creating static networks Trends Biotechnol 34 733–45 [PubMed: 27032730]

[12]. Dan P, Velot É, Decot V and Menu P 2015 The role of mechanical stimuli in the vascular differentiation of mesenchymal stem cells J. Cell Sci 128 2415–22 [PubMed: 26116570]

Author Manuscript Author Manuscript Author Manuscript Author Manuscript

[13]. Miller CJ and Davidson LA 2013 The interplay between cell signalling and mechanics in developmental processes Nat. Rev. Genet 14 733–44 [PubMed: 24045690]

[14]. Lee YJ, Lee HJ, Choi SH, Jin YB, An HJ, Kang JH, Yoon SS and Lee YS 2012 Soluble HSPB1 regulates VEGF-mediated angiogenesis through their direct interaction Angiogenesis 15 229–42 [PubMed: 22350794]

[15]. Sawada J, Li F and Komatsu M 2016 R-Ras inhibits VEGF-induced p38MAPK activation and HSP27 phosphorylation in endothelial cells J. Vasc. Res 52 12

[16]. Yuno A, Lee MJ, Lee S, Tomita Y, Rekhtman D, Moore B and Trepel JB 2018 Clinical evaluation and biomarker profiling of Hsp90 inhibitors Methods Mol. Biol 1709 18

[17]. Schilling D, Garrido C, Combs SE and Multhoff G 2017 The Hsp70 inhibiting peptide aptamer A17 potentiates radiosensitization of tumor cells by Hsp90 inhibition Cancer Lett 390 146–52 [PubMed: 28108313]

[18]. A R J, Gutierrez DA, DeJesus RE, Contreras L, Rodriguez-Palomares IA, Villanueva PJ, Balderrama KS, Monterroza L, Larragoity M and Varela-Ramirez A 2019 A new pyridazinone exhibits potent cytotoxicity on human cancer cells via apoptosis and poly-ubiquitinated protein accumulation Cell Biol. Toxicol 35 17

[19]. Iglesias-Figueroa BF, Siqueiros-Cendón TS, Gutierrez DA, Aguilera RJ, Espinoza-Sánchez EA, Arévalo-Gallegos S, Varela-Ramirez A and Rascón-Cruz Q 2019 Human recombinant lactoferrin induces apoptosis, disruption of F-actin structure and cell cycle arrest with selective cytotoxicity on human triple negative breast cancer cells Apoptosis 24 1–16 [PubMed: 30612317]

[20]. Varela-Ramirez A, Costanzo M, Carrasco YP, Pannell KH and Aguilera RJ 2011 Cytotoxic effects of two organotin compounds and their mode of inflicting cell death on four mammalian cancer cells Cell Biol. Toxicol 27 159–68 [PubMed: 21069563]

[21]. Ruiz-Medina BE, Lerma D, Hwang M, Ross JA, Skouta R, Aguilera RJ, Kirken R, Varela-Ramirez A and Robles-Escajeda E 2019 Green barley mitigates cytotoxicity in human lymphocytes undergoing aggressive oxidative stress, via activation of both the Lyn/PI3K/Akt and MAPK/ERK pathways Sci. Rep 9 1–11 [PubMed: 30626917]

[22]. Robles-Escajeda E, Lerma D, Nyakeriga AM, Ross JA, Kirken RA, Aguilera RJ and Varela-Ramirez A 2013 Searching in mother nature for anti-cancer activity: anti-proliferative and pro-apoptotic effectelicited by green barley on leukemia/lymphoma cells PLoS One 8 1–18

[23]. Segawa K and Nagata S 2015 An apoptotic 'Eat Me' signal: phosphatidylserine exposure Trends Cell Biol 25 639–50 [PubMed: 26437594]

[24]. Robles-Escajeda E, Das U, Ortega NM, Parra K, Francia G, Dimmock JR, Varela-Ramirez A and Aguilera RJ 2016 A novel curcumin-like dienone induces apoptosis in triple-negative breast cancer cells Cell Oncol. (Dordr) 39 265–77 [PubMed: 26920032]

[25]. Villanueva PJ, Martinez A, Baca ST, DeJesus RE, Larragoity M, Contreras L, Gutierrez DA, Varela-Ramirez A and Aguilera RJ 2018 Pyronaridine exerts potent cytotoxicity on human breast and hematological cancer cells through induction of apoptosis PLoS ONE 13 1–18

[26]. Contreras L, Calderon RI, Varela-ramirez A, Zhang H and Quan Y 2018 Induction of apoptosis via proteasome inhibition in leukemia/lymphoma cells by two potent piperidones Cell Oncol. (Dordr) 41 623–36 [PubMed: 30088262]

[27]. Brana C, Benham C and Sundstrom L 2002 A method for characterising cell death *in vitro* by combining propidium iodide staining with immunohistochemistry Brain Res. Protocols 10 109–14

[28]. Nicolau Y, Bany-Mohammed F, Cai CL, Aranda JV and Beharry KD 2018 SiRNA silencing of VEGF, IGFs, and their receptors in human retinal microvascular endothelial cells Am. J. Transl. Res 10 1990–2003 [PubMed: 30093937]

[29]. Kaplan O, Zárubová J, Mikulová B, Filová E, Bártová J, Bačáková L and Brynda E 2016 Enhanced mitogenic activity of recombinant human vascular endothelial growth factor VEGF121 expressed in E. coli origami B (DE3) with molecular chaperones PLoS ONE 11 1–22

[30]. Cui X, Boland T, D'Lima DD and Lotz MK 2012 Thermal inkjet printing in tissue engineering and regenerative medicine. Recent Pat. Drug Deliv. Formulation 6 149–55

[31]. Tay, BY; Queen Mary University. Continuous direct ink jet printing. 2001. Thesis

[32]. Weber A, Wasiliew P and Kracht M 2010 Interleukin-1 (IL-1) Pathway Sci. Signal 3 1–7

Author Manuscript Author Manuscript Author Manuscript Author Manuscript

[33]. Henderson B and Kaiser F 2013 Do reciprocal interactions between cell stress proteins and cytokines create a new intra-/extra-cellular signalling nexus? Cell Stress Chaperones (10.1007/s12192-013-0444-9)

[34]. dela Paz NG, Walshe TE, Leach LL, Saint-Geniez M and D'Amore PA 2012 Role of shear-stress-induced VEGF expression in endothelial cell survival J. Cell Sci (10.1242/jcs.084301)

[35]. Kishor A, Tandukar B, Ly YV, Toth EA, Suarez Y, Brewer G and Wilson GM 2013 Hsp70 is a novel posttranscriptional regulator of gene expression that binds and stabilizes selected mRNAs containing AU-Rich Mol. Cell Biol 33 71–84 [PubMed: 23109422]

[36]. Waugh DJJ and Wilson C 2008 The interleukin-8 pathway in cancer Clin. Cancer Res 14 6735–41 [PubMed: 18980965]

[37]. Ning Y et al. 2011 Interleukin-8 is associated with proliferation, migration, angiogenesis and chemosensitivity *in vitro* and *in vivo* in colon cancer cell line models Int. J. Cancer 128 2038–49 [PubMed: 20648559]

[38]. Martin D, Galisteo R and Gutkind JS 2009 CXCL8/IL8 stimulates vascular endothelial growth factor (VEGF) expression and the autocrine activation of VEGFR2 in endothelial cells by activating NFκB through the CBM (Carma3/Bcl10/Malt1) complex J. Biol. Chem 284 6038–42 [PubMed: 19112107]

[39]. Moon WS, Rhyu KH, Kang MJ, Lee DG, Yu HC, Yum JH, Koh GY and Tarnawski AS 2003 Overexpression of VEGF and angiopoietin 2: a key to high vascularity of hepatocellular carcinoma? Mod Pathol 1 1–6

[40]. Yoshiji H et al. 2005 Angiopoietin 2 displays a vascular endothelial growth factor dependent synergistic effect in hepatocellular carcinoma development in mice Gut 54 1768–75 [PubMed: 16033879]

[41]. Fagiani E and Christofori G 2013 Angiopoietins in angiogenesis Cancer Lett 328 18–26 [PubMed: 22922303]

[42]. Kim TK, Na HJ, Lee WR, Jeoung MH and Lee S 2016 Heat shock protein 70–1A is a novel angiogenic regulator Biochem. Biophys. Res. Commun 469 222–8 [PubMed: 26657847]

[43]. Park SL et al. 2017 HSP70–1 is required for interleukin-5-induced angiogenic responses through eNOS pathway Sci. Rep 7 1–14 [PubMed: 28127051]

[44]. Lieu C, Heymach J, Overman M, Tran H and Kopetz S 2011 Beyond VEGF: inhibition of the fibroblast growth factor pathway and antiangiogenesis Clin. Cancer Res 17 6130–9 [PubMed: 21953501]

[45]. Otrock ZK, Mahfouz RAR, Makarem JA and Shamseddine AI 2007 Understanding the biology of angiogenesis: review of the most important molecular mechanisms Blood Cells, Mol. Dis 39 212–20 [PubMed: 17553709]

[46]. Gowdak LHW and Krieger JE 2018 Vascular growth factors, progenitor cells, and angiogenesis Endothelium and Cardiovascular DiseasesVascular Biology and Clinical Syndromes ed Da Luz Protásio L. et al. (New York: Elsevier) ch 5 pp 49–62

[47]. Bartoli M, Gu X, Tsai NT, Venema RC, Brooks SE, Marrero MB and Caldwell RB 2000 Vascular endothelial growth factor activates STAT proteins in aortic endothelial cells J. Biol. Chem 275 33189–92 [PubMed: 10961983]

[48]. Gomez D and Reich NC 2003 Stimulation of primary human endothelial cell proliferation by IFN J. Immunol 170 5373–81 [PubMed: 12759411]

[49]. Werdich XQ and Penn JS 2006 Src, Fyn and Yes play differential roles in VEGF-mediated endothelial cell events Angiogenesis 8 315–26

[50]. Somanath PR, Razorenova OV, Chen J and Byzova TV 2006 Akt1 in endothelial cell and angiogenesis Cell Cycle 5 512–8 [PubMed: 16552185]

[51]. Farhan MA, Carmine-Simmen K, Lewis JD, Moore RB and Murray AG 2015 Endothelial cell mTOR complex-2 regulates sprouting angiogenesis PLoS ONE 10 1–20

[52]. Li P et al. 2018 Src plays an important role in AGE-induced endothelial cell proliferation, migration, and tubulogenesis Frontiers Physiol 9 1–14

[53]. Ahn J, Urist M and Prives C 2004 The Chk2 protein kinase DNA Repair 3 1039–47 [PubMed: 15279791]

Author Manuscript Author Manuscript Author Manuscript Author Manuscript

[54]. Zhao JX, Yue WF, Zhu MJ and Du M 2011 AMP-activated protein kinase regulates β-catenin transcription via histone deacetylase 5 J. Biol. Chem 286 16426–34 [PubMed: 21454484]

[55]. Koteswara Rao C, Mohammad T, Tiffany S and Dolly M 2011 Cyclic AMP response element-binding protein prevents endothelial permeability increase through transcriptional controlling p190RhoGAP expression Blood 119 308–19 [PubMed: 22049513]

[56]. McCubrey JA et al. 2014 GSK-3 as potential target for therapeutic intervention in cancer Oncotarget 5 2881–911 [PubMed: 24931005]

[57]. Ma J, Zhang L, Han W, Shen T, Ma C, Lui Y, Nie X, Lui M, Ran Y and Zhu D 2012 Activation of JNK/c-Jun is required for the proliferation, survival, and angiogenesis induced by EET in pulmonary artery endothelial cells J. Lipid Res 53 1093–105 [PubMed: 22493087]

[58]. Folkman J. 2004; Angiogenesis and C-Jun. J Natl Cancer Inst. 96:2115.

[59]. Uchida C, Gee E, Ispanovic E and Haas TL 2008 JNK as a positive regulator of angiogenic potential in endothelial cells Cell Biol Int 32 769–76 [PubMed: 18455449]

[60]. Santos-oliveira P, Correia A, Rodrigues T, Ribeiro-Rodrigues TM, Matafome P, Rodríguez-Manzaneque JC, Seiça R, Girão H and Travasso RD 2015 The force at the tip—modelling tension and proliferation in sprouting angiogenesis PLoS Comput Biol 11 1–20

[61]. Norton K and Popel AS 2016 Effects of endothelial cell proliferation and migration rates in a computational model of sprouting angiogenesis Sci. Rep 6 1–10 [PubMed: 28442746]

[62]. Miles KM et al. 2014 Dll4 blockade potentiates the anti-tumor effects of VEGF inhibition in renal cell carcinoma patient-derived xenografts PLoS One 9 1–11

[63]. Wu J, Liu T, Rios Z, Mei Q, Lin X and Cao S 2017 Heat shock proteins and cancer Trends Pharmacol. Sci (10.1016/j.tips.2016.11.009)

[64]. Batulan Z, Pulakazhi Venu VK, Li Y, Koumbadinga G, Alvarez-Olmedo DG, Shi C and O'Brien ER 2016 Extracellular release and signaling by heat shock protein 27: role in modifying vascular inflammation Frontiers Immunol 7 1–16

[65]. Thuringer D, Hébrard S, Bouchot A, Hazoumé A, Joly AL, Gleave M, Rosa-Calatrava M, Solary E and Garrido C 2013 Extracellular HSP27 mediates angiogenesis through Toll-like receptor 3 FASEB J 27 4169–83 [PubMed: 23804239]

[66]. O'Callaghan-Sunol C, Gabai VL and Sherman MY 2007 Hsp27 modulates p53 signaling and suppresses cellular senescence Cancer Res 67 11779–88 [PubMed: 18089808]

[67]. Lin CS, He PJ, Hsu WT, Wu MS, Wu CJ, Shen HW, Hwang CH, Lai YK, Tsai NM and Liao KW 2010 *Helicobacter pylori*-derived heat shock protein 60 enhances angiogenesis via a CXCR2-mediated signaling pathway Biochem. Biophys. Res. Commun 397 283–9 [PubMed: 20580690]

[68]. Pfister G, Stroh CM, Perschinka H, Kind M, Knoflach M, Hinterdorfer P and Wick G 2005 Detection of HSP60 on the membrane surface of stressed human endothelial cells by atomic force and confocal microscopy J. Cell Sci 118 1587–94 [PubMed: 15784682]

[69]. Reddy VS, Madala SK, Trinath J and Reddy GB 2018 Extracellular small heat shock proteins: exosomal biogenesis and function Cell Stress Chaperones 23 441–54 [PubMed: 29086335]

[70]. Caruso Bavisotto C, Cappello F, Macario AJL, Conway de Macario E, Logozzi M, Fais S and Campanella C 2017 Exosomal HSP60: a potentially useful biomarker for diagnosis, assessing prognosis, and monitoring response to treatment Expert Rev. Mol. Diagn 17 815–22 [PubMed: 28718351]

[71]. Guzhova IV, Shevtsov MA, Abkin SV, Pankratova KM and Margulis BA 2013 Intracellular and extracellular Hsp70 chaperone as a target for cancer therapy Int. J. Hyperth 29 399–408

[72]. Sun J and Liao JK 2004 Induction of angiogenesis by heat shock protein 90 mediated by protein kinase Akt and endothelial nitric oxide synthase Arterioscler. Thromb. Vasc. Biol 24 2238–44 [PubMed: 15486309]

[73]. Venkatesh S and Suzuki CK 2017 HSP60 takes a hit: inhibition of mitochondrial protein folding Cell Chem. Biol 24 543–5 [PubMed: 28525768]

[74]. van Beijnum JR, Buurman WA and Griffioen AW 2008 Convergence and amplification of toll-like receptor (TLR) and receptor for advanced glycation end products (RAGE) signaling pathways via high mobility group B1 (HMGB1) Angiogenesis 11 91–9 [PubMed: 18264787]

[75]. Schiele NR, Corr DT, Huang Y, Raof NA, Xie Y and Chrisey DB 2010 Laser-based direct-write techniques for cell printing Biofabrication 2 1–14

Author Manuscript Author Manuscript Author Manuscript Author Manuscript

[76]. Townsend-Nicholson A and Jayasinghe SN 2006 Cell electrospinning: a unique biotechnique for encapsulating living organisms for generating active biological microthreads/scaffolds Biomacromolecules 7 3364–9 [PubMed: 17154464]

[77]. Canbolat MF, Tang C, Bernacki SH, Pourdeyhimi B and Khan S 2011 Mammalian cell viability in electrospun composite nanofiber structures Macromol Biosci 11 1346–56 [PubMed: 21984502]

[78]. Sarker MD, Naghieh S, Sharma NK and Chen X 2018 3D biofabrication of vascular networks for tissue regeneration: a report on recent advances J. Pharm. Anal 8 277–96 [PubMed: 30345141]

Author Manuscript Author Manuscript Author Manuscript Author Manuscript

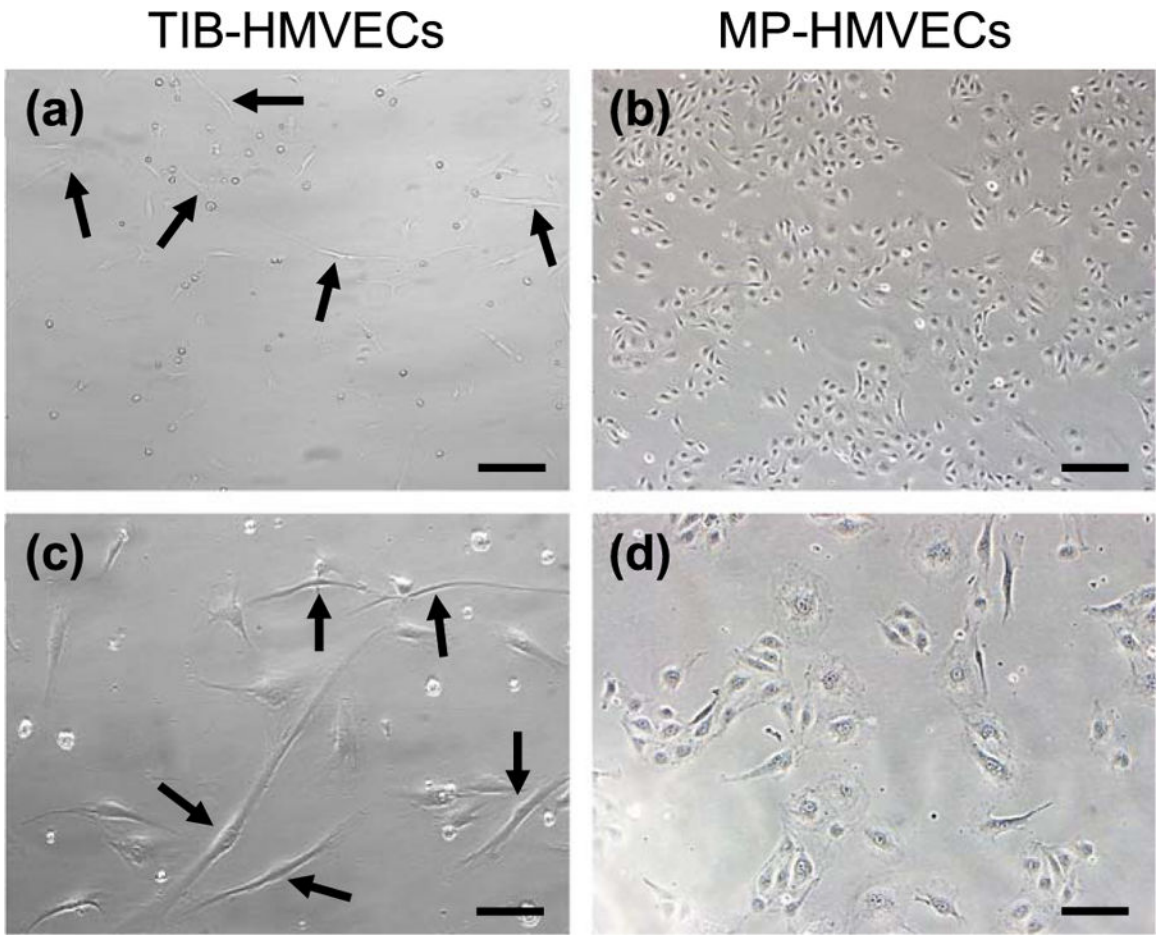

Figure 1.

Cell morphology between TIB and MP HMVECs after a 24 h incubation period. (a) and (c) demonstrate TIB-HMVECs at 10× and 20×, respectively. Arrows indicate elongated cells. Images (b) and (d) show MP-HMVECs at 10× and 20×, respectively. Their appearance is almost diamond-shaped with some cells demonstrating minor elongation. TIB = thermal inkjet bioprinted. MP = manually pipetted, HMVECs = human microvascular endothelial cells, Scale bar 10× = 100 μm and 20× = 200 μm.

Author Manuscript Author Manuscript Author Manuscript Author Manuscript

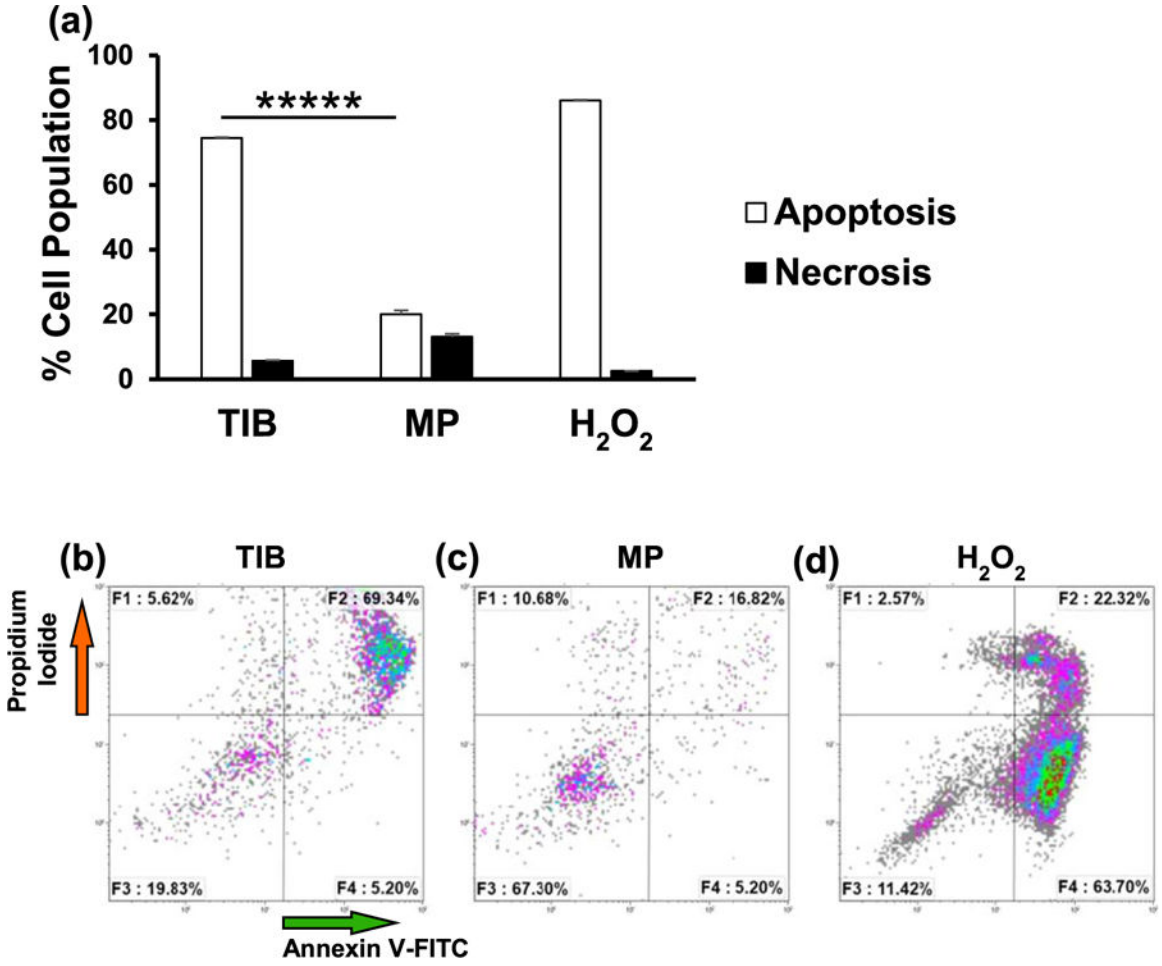

Figure 2.

Flow cytometry analysis demonstrating phosphatidylserine (PtdSer) externalization for TIB and MP HMVECs after a 24 h incubation period. F1 quadrant represents necrotic cells (PI positive and annexin negative). F2 quadrant represents cells that are in late apoptosis (both PI and annexin positive). F3 quadrant represents viable cells (both annexin and PI negative). F4 represents cells in early apoptosis (annexin positive and PI negative). (a) Bar graph demonstrating the differences in percentage rates of apoptosis and necrotic cells among TIB and MP HMVECs. The total percent of apoptotic cells is expressed as the sum of the early and late stages of apoptosis (white bars), as determined by the percentage of annexin V-FITC positive cells. Each bar represents the average of three independent measurements and the error bars represent their corresponding standard deviations. Dot plots show ratios of apoptosis among TIB-HMVECs. (b) Dot plots show ratios of apoptosis in TIB-HMVECs. (c) Dot plots show ratios of apoptosis in MP-HMVECs. (d) Dot plots show apoptosis of positive control (HMVECs in 1 mM H_2O_2). TIB = thermal inkjet bioprinted, MP = manually pipetted, HMVECs = human microvascular endothelial cells. ***** $P < 0.000\ 01$.

Author Manuscript Author Manuscript Author Manuscript Author Manuscript

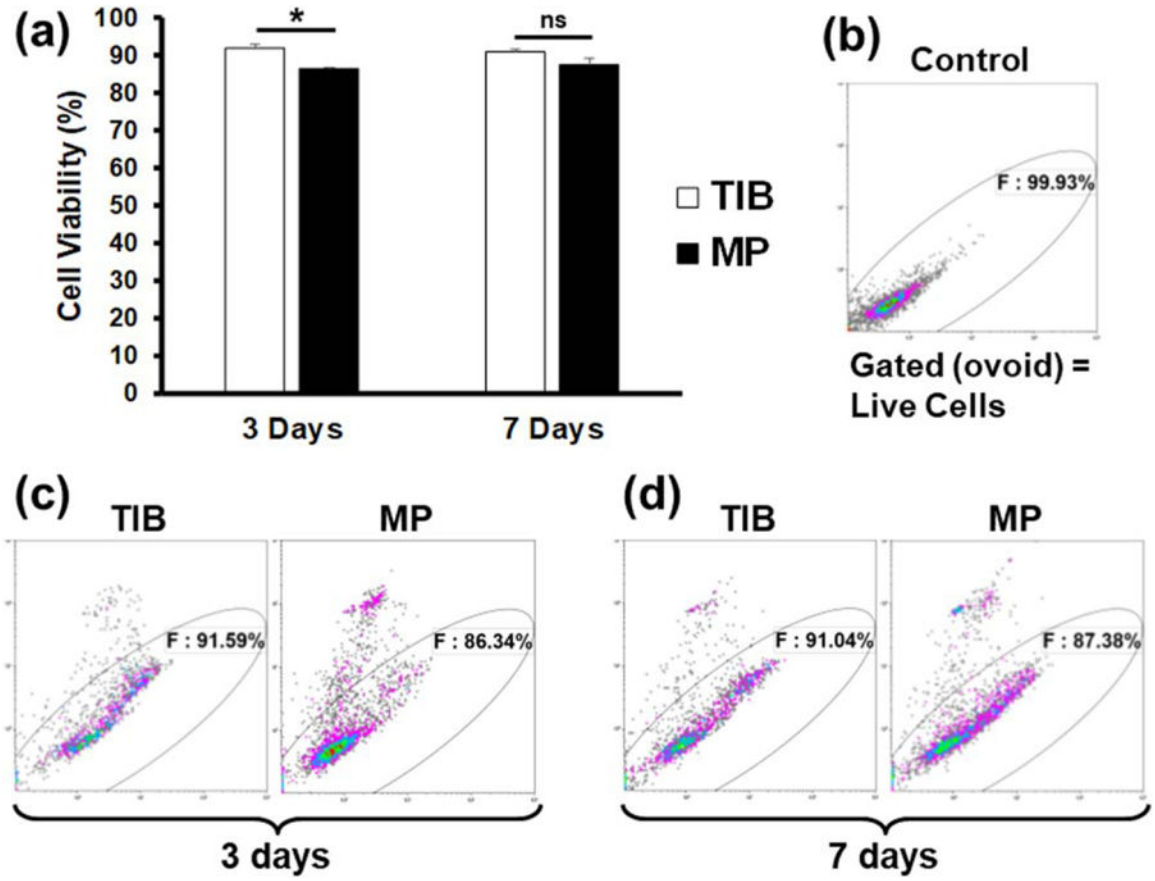

Figure 3.

Flow cytometry analysis of a PI exclusion assay demonstrating cell viability percentages between TIB and MP-HMVECs at 3 and 7 d incubation periods. (a) Bar graph depicting the differences in cell viability by percent among TIB and MP-HMVECs. Each bar represents the average of three independent measurements and the error bars represent their corresponding standard deviations. (b) Flow cytometric dot plot of untreated HMVECs without PI used to demark the gate of viable cells. (c) Dot plots demonstrating the differences in cell viability by percent between TIB and MP-HMVECs at a 3 d incubation period. (d) Dot plot showing the differences in cell viability by percent between TIB and MP-HMVECs at a 7 d incubation period. PI = propidium iodide, TIB = thermal inkjet bioprinted, MP = manually pipetted, HMVECs = human microvascular endothelial cells, ns = no significant difference. $*P < 0.05$.

Author Manuscript Author Manuscript Author Manuscript Author Manuscript

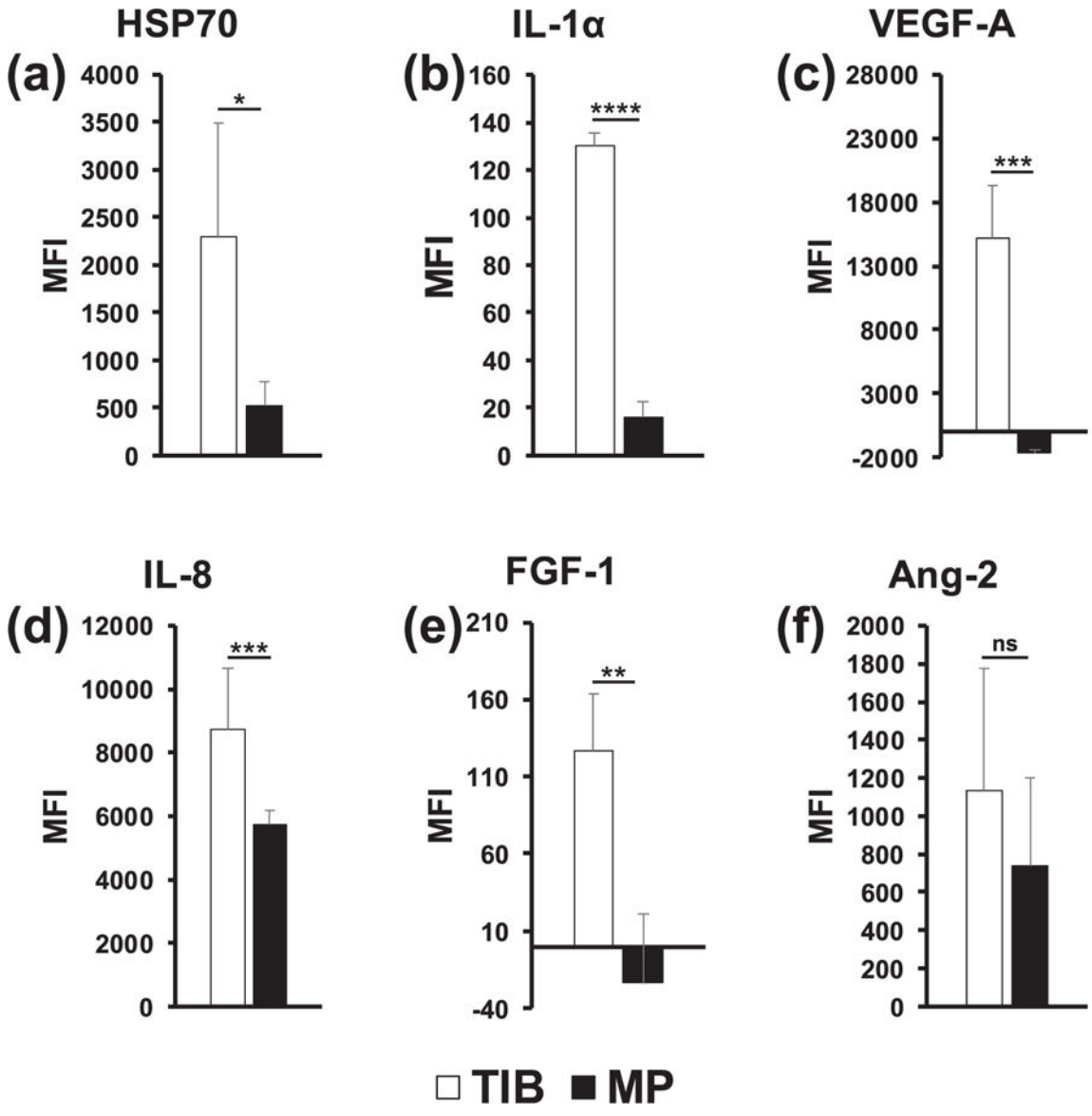

Figure 4.

In vitro Milliplex magnetic bead panel analysis of 6 specifically selected cytokines after a 12 h incubation period. (a) HSP70 was significantly overexpressed in TIB-HMVECs as compared to MP-HMVECs. (b) IL-1α was significantly overexpressed among TIB-HMVECs in comparison to MP-HMVECs. (c) VEGF-A was significantly overexpressed in TIB-HMVECs as compared to MP-HMVECs. (d) IL-8 was significantly overexpressed in TIB-HMVECs as compared to MP-HMVECs. (e) FGF-1 was significantly overexpressed among TIB-HMVECs in comparison to MP-HMVECs. (f) Ang-2 demonstrated no significant differences in expression between TIB and MP-HMVECs. HSP70 = heat-shock protein 70, IL-1α = interleukin 1α, VEGF-A = vascular endothelial growth factor A, IL-8 = interleukin 8, FGF-1 = fibroblast growth factor 1, Ang-2 = Angiopoietin 2, TIB = thermal inkjet bioprinted, MP = manually pipetted, HMVECs = human microvascular endothelial

cells, MFI = median fluorescent intensity, ns = no significant difference. *$P < 0.05$; **$P < 0.01$; ***$P < 0.001$; ****$P < 0.0001$.

Author Manuscript Author Manuscript Author Manuscript Author Manuscript

Author Manuscript Author Manuscript Author Manuscript Author Manuscript

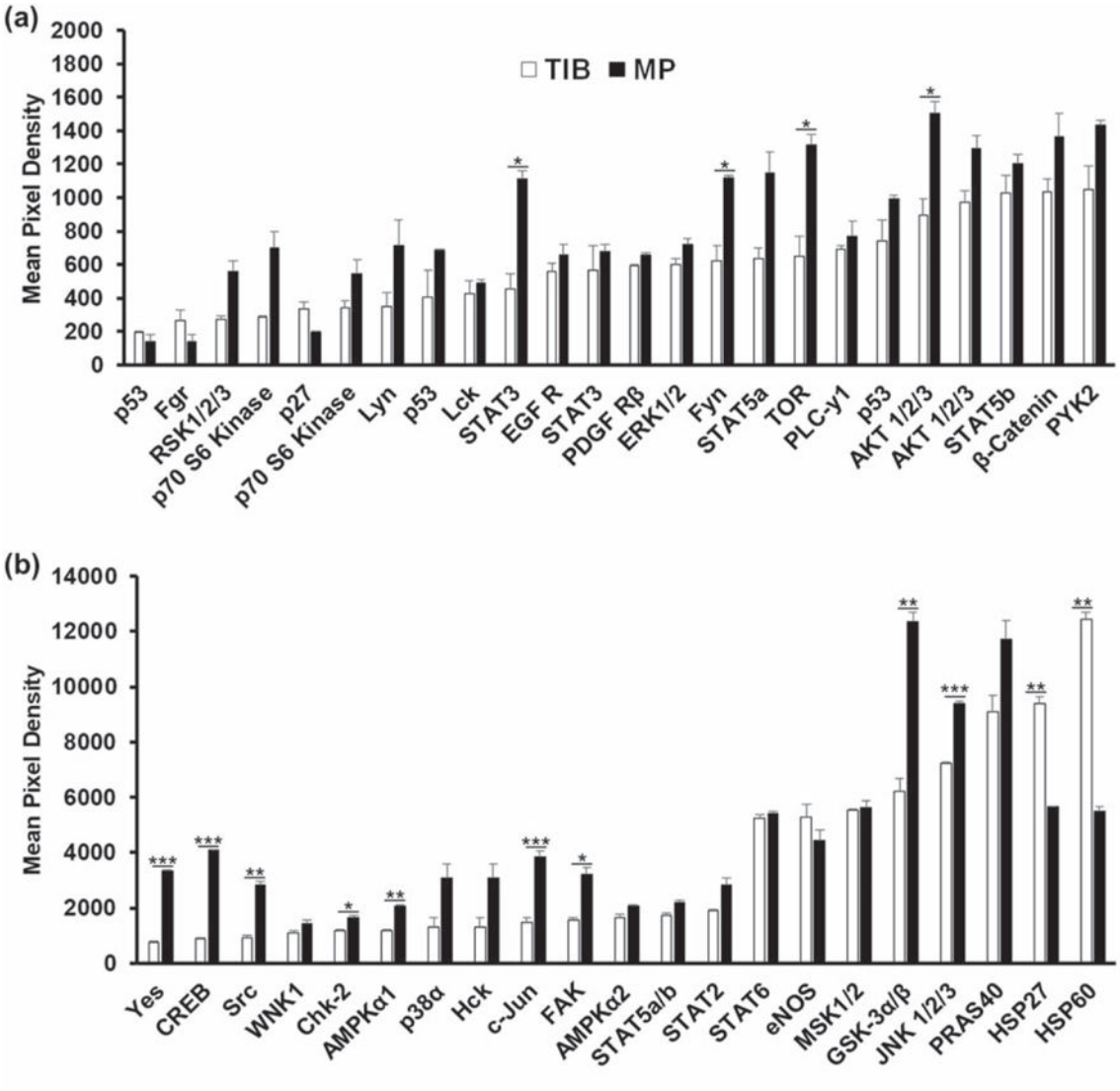

Figure 5.

In vitro human phospho-kinase array analysis of the activation of 45 kinases in HMVECs after a 12 h incubation period. (a) STAT3, Fyn, TOR, AKT 1/2/3 were significantly overactivated among MP-HMVECs as compared to TIB-HMVECs.(b) Yes, CREB, Src, Chk-2, AMPKα1, c-JUN, FAK, GSK-3α/β, and JNK 1/2/3 were significantly overactivated among MP-HMVECs as compared to TIB-HIMVECs while HSP27 and HSP60 were overactivated significantly in TIB-HMVECs in comparison MP-HMVECs. STAT = signal transducer and activator of transcription proteins, EGF R = epidermal growth factor receptor, PDGF R = platelet-derived growth factor receptor, AKT = protein kinase B, PYK-2 = proline-rich tyrosine kinase 2, CREB = cAMP response element-binding protein, WNK1 = lysine deficient protein kinase 1, AMPK = adenosine monophosphate-activated protein kinase, eNOS = endothelial nitric oxide synthase, MSK = mitogen- and stress-activated protein kinase, GSK = glycogen synthase kinase, JNK = Jun N-terminal kinase, PRAS = proline-rich AKT substrate, HSP = heat-shock protein, TIB = thermal inkjet bioprinted, MP

= manually pipetted, HMVECs = human microvascular endothelial cells. *$P < 0.05$; **$P < 0.01$; ***$P < 0.001$.

Author Manuscript Author Manuscript Author Manuscript Author Manuscript

Author Manuscript Author Manuscript Author Manuscript Author Manuscript

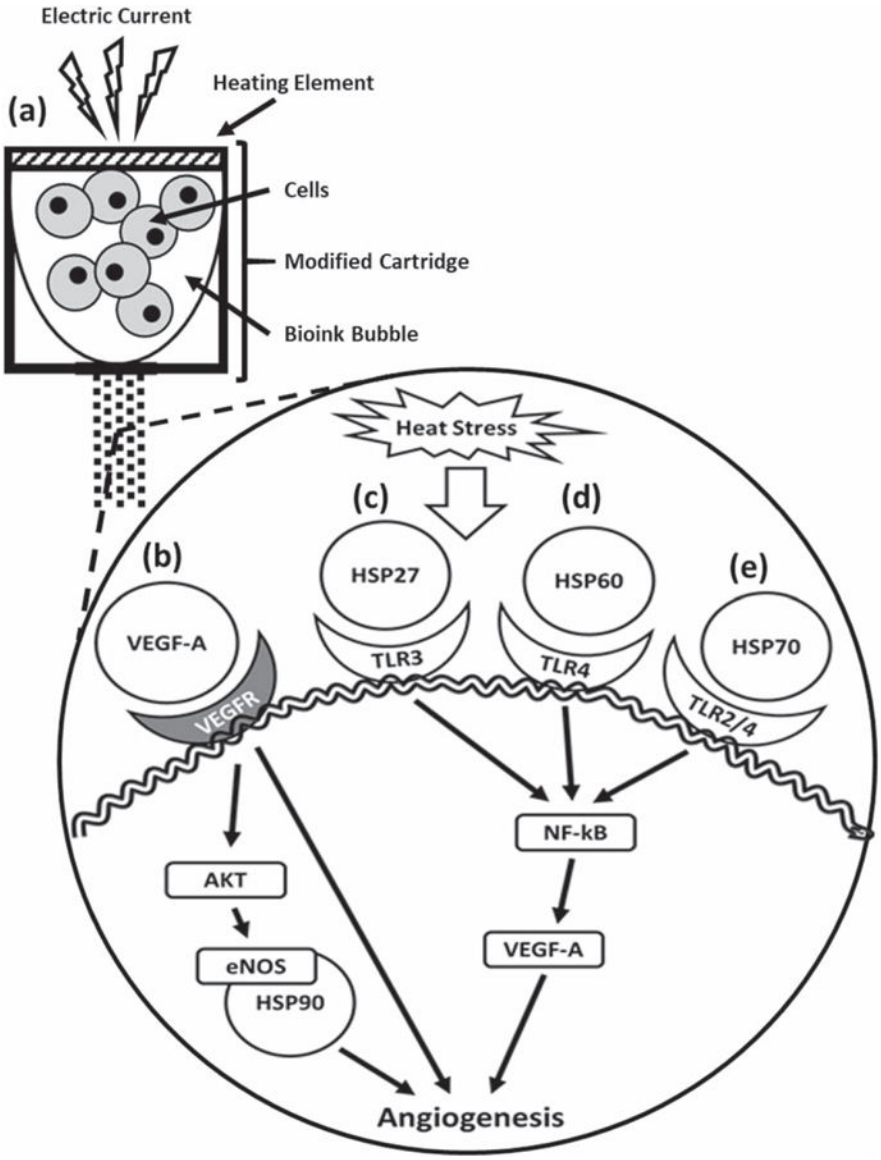

Figure 6.

Schematic of how thermal inkjet bioprinting triggers the activation of the VEGF pathway. Heat from the printing process causes cellular heat stress leading to various pathways in which extracellular heat-shock proteins play an angiogenic role. (a) The electric current heats a heating element producing a bubble that collapses causing the ejection of droplets containing cells. (b) VEGF-A binds VEGFR and either activates the AKT-eNOS-HSP90 pathway or promotes angiogenesis directly [72]. (c) HSP27 binds the TLR-3 activating the NF-κB pathway to produce VEGF and induce angiogenesis [64]. (d) Mitochondrial HSP60 binds the TLR-4 [68] leading to the activation of angiogenesis [63, 73]. (e) HSP70 binds TLR 2 and TLR-4 [71] leading to the activation of the NF-κB pathway to produce VEGF and induce angiogenesis [64, 74]. HSP = heat-shock protein, VEGFR = vascular endothelial growth factor receptor, eNOS = endothelial nitric oxide synthase, TLR = toll-like receptor, NF-κB = nuclear factor kappa-light-chain-enhancer of activated B cells.